Original Article

The Possible Ameliorating Role of Platelet Rich Plasma versus Propolis on Submandibular Salivary Glands Damage Induced by Methotrexate in Adult Male Albino rats (Light and Transmission Electron Microscopic Study)

Rania Osama M. Mohsen and Hend El-Messiry

Department of Oral Biology, Faculty of Dentistry, Ain Shams University, Cairo, Egypt

ABSTRACT

Introduction: Methotrexate (MTX) has been widely used as an effective chemotherapeutic agent, but because of its side effects, there is a continuous intention to lessen its toxicity. MTX has muco-toxic effects on salivary gland causing dysfunction. Platelet rich plasma (PRP) is an economical and autogenous source of growth factors used in tissue repair. Natural product as propolis is considered as an alternative medical tool that has great effect on human health.

Aim of the Work: To examine the effect of PRP versus propolis on submandibular salivary glands (SMSG) in rats given MTX.

Material and Method: 28 male Albino rats weighting 100-150 g, were divided equally into four groups; Control group (Gp I): rats received no drugs. MTX group (Gp II): The rats were given a single intraperitoneal injection of MTX (80 mg/Kg). PRP treated MTX group (Gp III): The rats received MTX as group II, then after 48 h, the rats were given a single subcutaneous injection of PRP (0.5 ml/kg). Propolis treated MTX group (Gp IV): The rats received MTX as group II, then after 48 h, the rats were given orally a single daily dose of propolis (300 mg/kg). After six days from MTX injection, half of SMSG specimens were processed and stained by Hematoxylin & Eosin (H&E) and Anti-Caspase 3. The other half of specimens were examined by transmission electron microscope (TEM).

Results: SMSG of Gp II showed significant histological and ultrastructure alterations with significant increase in area percentage of positive reaction to Anti-Caspase 3 compared to Gp I. In treated groups, Gp III & Gp IV, SMSG showed histological and ultrastructure improvements with significant decrease in area percentage of positive reaction to Anti-Caspase 3 compared to Gp II.

Conclusion: Administration of PRP and propolis with MTX have effective therapeutic strategy in improving the detrimental effects of MTX on SMSG.

Received: 03 February 2022, **Accepted:** 19 March 2022

Key Words: Anti-Caspase 3; MTX; PRP; propolis; TEM.

Corresponding Author: Rania Osama M. Mohsen, PhD, Department of Oral Biology, Faculty of Dentistry, Ain-Shams University, Cairo, Egypt, **Tel.**: +20 10 0364 0858, **E-mail:** dr.rania.osama@dent.asu.edu.eg

ISSN: 1110-0559, Vol. 46, No. 2

INTRODUCTION

Chemotherapy aims to cause lethal cytotoxic effect in cancer cells, arresting tumors progression. Unfortunately, most currently available anticancer drugs not interfere only with cellular processes unique to malignant cells, but also affect the normal cells. Methotrexate (MTX) is widely used as a cytotoxic chemotherapeutic agent in treatment of several malignancies and certain inflammatory diseases. MTX is related to folic acid structurally and acts as its antagonist, inhibiting dihydrofolate reductase enzyme. This action prevents the conversion of folic acid to its active form, leading to depressed DNA, RNA and protein synthesis with subsequent apoptotic cell death[1].

Major salivary glands secrete about 90% of daily saliva that provides lubrication, antibacterial, antifungal and anti-inflammatory functions through its components. The malfunction of salivary glands causes changes in the composition and decrease in the amount of saliva which leads to dry mouth (xerostomia). Xerostomia can be clinically manifested by oral mucositis. Oral mucositis is one of the common side effects caused by chemotherapeutic drugs, affecting the patient quality of life, reducing the drug dose and delaying the treatment completion. It was proven that MTX caused such malfunction which aggravated its secondary muco-toxic effects[2].

The systemic oxidative stress is an important factor in the MTX-induced toxicity. MTX results in increasing the level of Malondialdehyde, the most significant indicator of membrane lipid peroxidation, which arises from the interaction of reactive oxygen species (ROS) with cellular membranes. Besides, MTX affects the antioxidant defense system by significantly reducing the Glutathione levels that results in accumulation of ROS and free radicals, leading to apoptotic cell death[3,4].

Apoptosis has a significant role in development and maintenance of multicellular organisms that involved in physiological, toxicological and pathological events. Apoptotic cell death is characterized by fragmentation of

 DOI: 10.21608/ejh.2022.119924.1639

DNA, nuclear shrinkage, chromatin condensation, cell shrinkage and fragmentation, forming apoptotic bodies. Apoptotic cell death is mediated by a cascade of proteolytic event where the caspases (a family of cysteine proteases) play a fundamental role in the initiation, regulation and execution that occur during apoptosis. Caspase 3 is one of the executioners involved in apoptosis that is necessary for large number of proteins cleavage and DNA fragmentation. Therefore, activated caspase 3 detection could be specific and valuable tool for apoptotic cells identification in tissue sections[5].

Platelet rich plasma (PRP) is a low-cost procedure to deliver high concentration of autologous growth factors, cytokines and cell adhesion molecules. Upon platelets activation, these factors are released, improving the physiological microenvironment at the site of injury or surgery, promoting tissue repair and wound regeneration, modulating the immune response and having antimicrobial action[6,7,8,9]. Hence, PRP represents a relatively advanced therapeutic approach in regenerative medicine for treatment of many serious diseases as diabetes[10], lithium induced thyroid follicular cell toxicity[11], cyclophosphamide (Cy)-induced ovarian damage[12]. Some studies reported that the growth factors released from the platelets would likely induce angiogenesis, stem cell differentiation and stimulate tumor growth as well as tissue regeneration[13]. However, others reported that PRP are very useful in cancer treatment when administrated with radiotherapy or used alone[14].

Nowadays as an alternative medical therapy, an obvious concern has been offered for utilizing the natural products that may have many pharmaceutical benefits. Propolis is mainly composed of plant resinous secretions that mixed with bees salivary and enzymatic secretions. In propolis, hundreds of compounds have been identified such as, phenolic compounds, essential oils, aromatic acids, amino acids and waxes. The use of propolis has great effect on human health that possesses many beneficial biological and pharmacological properties, such as anti-bacterial, anti-inflammatory, anti-viral, anti-oxidant, anti-cancer and anti-mutagenic properties[15,16]. Several researchers have focused in their experiments on the biological activity of propolis especially its antioxidant property to modulate a variety of diseases and toxicity in animals as diabetic hepatotoxicity[17], Osteoporosis[18], MTX-induced stress in liver and brain[19] and aluminum silicate intoxication[20].

The aim of this study was to investigate the possible ameliorating effect of PRP and propolis on the histological structure of submandibular salivary glands (SMSG) in rats given MTX.

MATERIALS AND METHODS

Chemicals

Primary antibody (polyclonal primary rabbit anti-Caspase 3, Cat. # 9662S) was purchased from (Cell Signaling Technology, Inc., Beverly, MA, USA), Secondary antibody (biotinylated goat anti-rabbit IgG, Cat. # SC-2040) from (Santa Cruz Biotechnology, Inc., Dallas, USA), Streptavidin horseradish-peroxidase complex (31491) from (Thermo Fisher Scientific Inc., Waltham, MA, USA), Diaminobenzidine plus chromogen (DAB) (ab64264) from (Abcam, Cambridge, MA, USA), MTX was supplied by (Mylan Pharmaceutical Industry Company, USA), Propolis from (Sigma Pharmaceutical Industries, Egypt), Sodium citrate anticoagulant (S5770), Phosphate buffered saline (PBS) (P5493), Calcium chloride (CaCl2) (499609), Hydrogen peroxide (H2O2) (88597), Hematoxylin (H3136), Citrate buffer (C9999), Osmium tetra-oxide (75632) and Toluidine blue (89640) were obtained from (Sigma Aldrich, St, Louis, MO, USA).

Preparation of PRP

Preparation of PRP was made using double centrifugation tube method. Two ml of fresh blood from the jugular vein was taken from 20 adult male rats. The blood was collected immediately into tubes that contained 0.3 ml of sodium citrate anticoagulant (3.2%). These tubes were then centrifuged at 1600 revolutions per minute (rpm) for 10 min. This resulted in the formation of three components of different densities; the superior layer that contained plasma and platelets, the middle layer that contained buffy coat of white blood cells and the inferior layer which contained red blood cells (RBSCs). The plasma was obtained by an automatic pipette then it was moved to another tube that was again centrifuged at 2000 rpm for 10 min. Two portions were obtained from plasma centrifugation: the upper one, which contained the platelet-poor plasma (PPP) and the lower portion which contained the platelet button. The PPP was then removed, and platelet button was gently agitated and resuspended in PBS (1:1). Platelets were finally counted using an automatic analyzer and platelet count was confirmed to be greater than 1,000,000/µl. Immediately before use, PRP activation were done by using 10% CaCl2 (0.8 ml PRP + 0.2 ml 10% CaCl2)[11].

Animals

Twenty-eight adult male Albino rats weighing between 100-150 g were used in this study. Throughout the whole experimental period, the rats were all housed in the animal house of Ain-Shams University in the “The Medical Research Center” and were then maintained in a sterile, controlled environment at a temperature (23±5°C), with dark/light cycles of 12 h and a free access to tap water and a standard pellet diet. The experimental protocol was then approved by the “Research Ethics Committee” of faculty of Dentistry, Ain Shams University, Cairo, Egypt, (Approval number: FDASU-Rec R102108). This experiment was performed in accordance with the guide of care and use of laboratory animals[21].

Experimental groups

Rats were randomly divided into four groups (7 rats in each group):

Control group (Gp I): rats received no drugs.

MTX group (Gp II): rats were given a single injection of MTX intraperitoneally (80 mg/Kg)[3].

PRP treated MTX group (Gp III): The rats received MTX as group II, then after 48 h, the rats were given a single subcutaneous injection of PRP (0.5 ml/kg) dissolved in PBS (PRP 1:1 PBS)[11].

Propolis treated MTX group (Gp IV): The rats received MTX as group II, then after 48 h, the rats were given orally a single daily dose of propolis (300 mg/kg) suspended in 1 ml distilled water[18].

Sample preparation

After six days from MTX injection[2], rats were sacrificed separately by an over dose of general anesthesia and both SMSG were immediately dissected, processed and examined using:

Light microscope (LM)

SMSG specimens were properly cut and immediately fixed in a solution of 10% phosphate buffered formalin for two days. The specimens were washed under running water after that dehydrated by transferring them through increasing alcohol concentrations. To clear specimens from alcohol, they were transferred to xylene. They were infiltrated with paraffin and then embedded in the center of the paraffin wax blocks. Sections of 4 µm thick were put in xylene and transferred into decreasing concentrations of alcohol then distilled water to remove paraffin wax[22]. Finally, the sections were finally stained by Hematoxylin & Eosin (H&E) and Anti-Caspase 3.

Immunohistochemical staining using Anti-Caspase 3

After performing deparaffinization and rehydration of sections, blocking endogenous peroxidase activity was done by incubating the specimen in 10% hydrogen peroxide (H2O2) in filtered water for 10-15 min. For antigen retrieval, sections were then microwaved with 10 mmol/L citrate buffer (pH 7) for 10 min, followed by incubating the sections with polyclonal primary rabbit Anti-Caspase 3 for 60 min at room temperature. After washing the slides in PBS, the sections were incubated with a biotin-conjugated secondary antibody (biotinylated goat anti-rabbit IgG) then with streptavidin horseradish-peroxidase complex for 30 min at room temperature. The reactions became visible after immersion of the slides in DAB solution. The specimens were counterstained with Hematoxylin for 2-3 min and rinsed in distilled water. Dehydration was done in graded alcohol and cleared in xylene. Afterward the specimens were mounted and cover slips were put in place then examined under LM[23].

The photomicrographs of SMSG were captured at (40x) objective magnification using a digital video camera (TVO.5XC, Olympus, China) at Oral Biology Department, Faculty of Dentistry, Ain-Shams University, Cairo, Egypt.

Transmission electron microscope (TEM)

Before fixation, SMSG specimens were cut into small parts of 1 mm3 then fixed in glutaraldehyde in phosphate buffer with a pH 7.2 for 6 h. and then washed in three changes of PBS. After that, secondary fixation was done using 1% osmium tetra-oxide at 48°C for 1.5 h and rinsed in PBS. Dehydration of the specimens was done in graded series of ethanol for 10 min each. The specimens were cleared in propylene oxide and embedded in epoxy resin and semi-thin sections of 1 mm were cut and were stained using 1% toluidine blue. Samples were then examined using LM to detect the site to be studied using TEM. Ultrathin sections (80-90 nm) were cut with a diamond knife and stained by lead citrate and Uranyl acetate[24]. The electron microscopic study was done using a JEOL 1010 transmission electron microscope (Japan) at 80 Kv at "the Regional Center for Mycology and Biotechnology", Al-Azhar University, Cairo, Egypt.

Histomorphometric analysis

Image J software (Version 1.41a, NIH, USA) was used in this study for the histo-morphometric analysis of Anti-Caspase 3 immuno-stained sections. The image analysis system was used to measure the total area (area percentage %) of immuno-positive reaction.

Seven SMSG specimens from each group were selected. Five equal representative fields scattered in the specimen were chosen for representing proper Anti-Caspase 3 reaction. The fields were captured and images were transferred to the computer system for further analysis. Images were corrected manually for brightness and contrast. Sampling was done to select the areas of interest, while the excluded areas covered by white pixels. After that, the images were converted into 8-bit monochrome type then color thresholding was performed and area fraction was automatically measured (Figure 1).

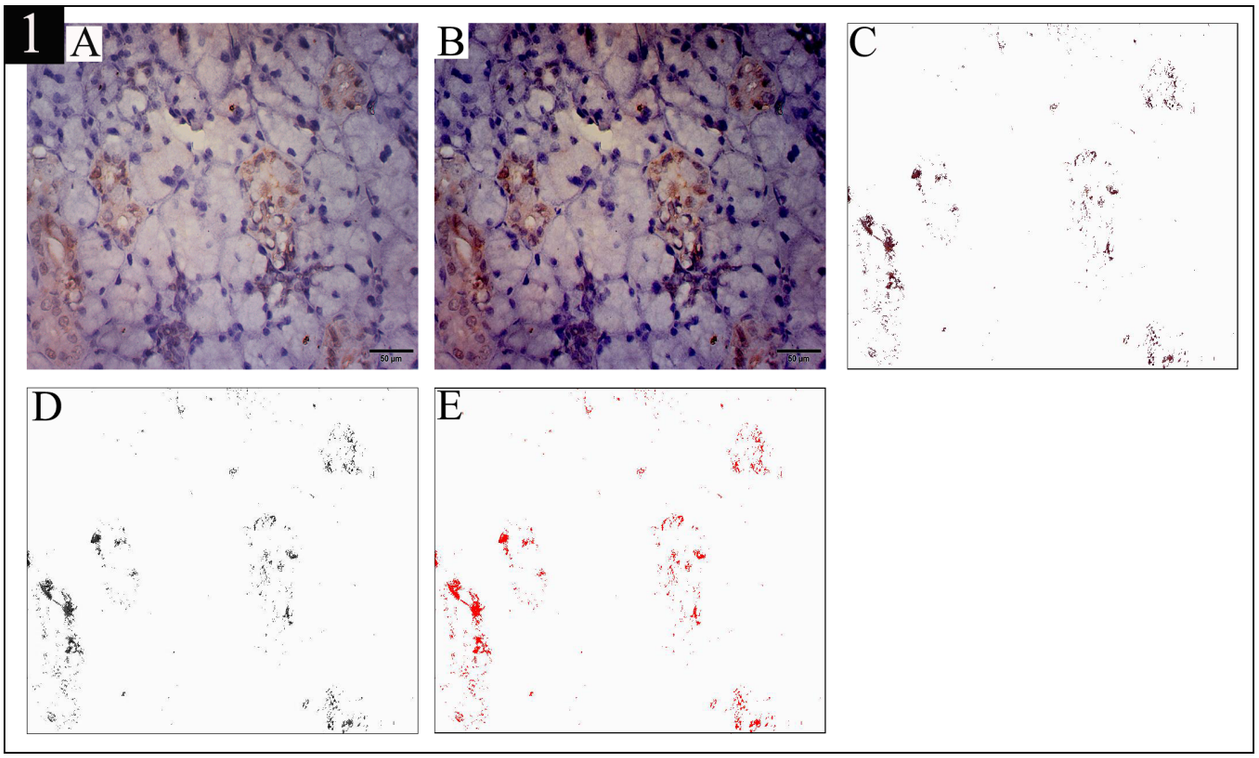

Fig. 1: Histomorphometric analysis: A: The original photomicrograph to be analyzed B: The photomicrograph after adjusting the brightness and contrast. C: An image where areas of interest were shown, while other areas were covered by white pixels. D: The image was converted to 8-bit monochrome type. E: Color thresholding was done to selected areas and labeled by red.

Statistical Analysis

Recorded data of area percentage (%) of positive reaction to Anti-Caspase 3 were analyzed using the statistical package for social sciences, version 23.0 (SPSS Inc., Chicago, Illinois, USA). The quantitative data were presented as mean ± standard deviation (SD) and ranges of their distribution. The following tests were done: Kruskall Wallis test for multiple-group comparisons in non-parametric data and Mann Whitney U test for two-group comparisons in non-parametric data. The confidence interval was set to 95% and the margin of error accepted was set to 5%. So, the probability *p-value* ≤ 0.05 was considered significant.

RESULTS

Light microscopic results for H&E stained sections

Gp I (Control group): Examination of this group showed normal architecture of the SMSG histologically (Figure 2). The serous acini appeared spherical in shape and was formed of pyramidal cells bordering a narrow lumen; the cells showed basophilic cytoplasm and basally situated rounded nuclei (Figure 2A). The gland showed intercalated ducts (ICDs) formed of cuboidal cells with basophilic cytoplasm and central rounded nuclei filling most of the cells (Figure 2B). The granular convoluted tubules (GCTs) were well defined kidney shaped and were lined by tall columnar cells and the nuclei were spherical and basally situated. Large eosinophilic granules were occupying the apical portion of the cells (Figure 2A). The striated ducts were lined by columnar cells with central nuclei. Cells showed basal striations and exhibited eosinophilic cytoplasm (Figure 2A). The excretory ducts were formed of pseudostratified columnar epithelium. Fibrous connective tissue (CT) stroma and blood vessels were seen surrounding the ducts (Figure 2C).

Gp II (MTX group): Examination of this group revealed that some serous acini showed degenerative changes in form of atrophy and acini were widely separated, nuclei of the acinar cells appeared hyperchromatic, pleomorphic and pyknotic in addition to presence of cytoplasmic vacuoles of varying sizes (Figures 3A,B,C). ICD appeared with apparent normal architecture but showed hyperchromatic nuclei and loss of cell height (Figure 3A). GCTs showed ill-defined outline, displacement and irregular arrangement of their nuclei with loss of their apical granules (Figure 3C). Striated ducts showed apparent decrease in cell height, displaced nuclei, apparent loss of basal striations and some showed stagnated secretion in their lumen (Figure 3A). Some excretory ducts appeared to be flattened with loss of pseudo-stratification in some areas of its lining as well as flattening of their cells and nuclei (Figure 3D). Presence of congested blood vessels and hyalinization in the surrounding CT. in some areas (Figure 3D).

Gp III (PRP treated MTX group): Serous cells and ICDs showed almost normal architecture (Figure 4A). GCTs exhibited apparently normal outline with apical eosinophilic granules and few pyknotic nuclei (Figure 4B). The striated ducts exhibited basal striations with few pyknotic crescent-shaped nuclei (Figure 4A). The excretory ducts showed pseudostratified epithelial lining. The ducts were surrounded by CT and associated with dilated and congested blood vessels (Figure 4C).

Gp IV (Propolis treated MTX group): Serous cells (Figure 5A) and ICDs (Figure 5B) showed almost normal architecture with presence of some extravasated RBCs between the acini. GCTs exhibited nearly normal outline with apical eosinophilic granules (Figure 5B). The striated ducts exhibited basal striations and few cytoplasmic vacuolations surrounded by congested blood vessel (Figure 5A). The excretory ducts showed pseudostratified epithelial lining and were surrounded by almost normal CT showing less hyalinization (Figure 5C).

Light microscopic results for immunohistochemical Anti-Caspase 3 stained sections

Anti-Caspase 3 stain was used to detect apoptosis and positive immunoreactivity was observed as brown discoloration predominantly in the cytoplasm with some nuclear staining.

Gp I: Examination of immuno-stained sections of this group revealed very few areas of positive reaction that seen in acinar and ductal cells (Figure 6A).

Gp II: Examination of this group showed obviously too many areas of positive reaction seen in both acinar and ductal cells (Figure 6B).

Gp III: The examination revealed few areas of positive reaction detected in acinar and ductal cells (Figure 6C).

Gp IV: Examination of immuno-stained sections showed very few areas of positive reaction in acinar and ductal cells (Figure 6D).

Transmission electron microscopic results

Gp I (Control group): Examination of the SMSG of Gp I showed normal architecture of acini and ducts (Figure 7). Acinar cells appeared as pyramidal cells with basal, spherical, vesicular nuclei, intact cell boundaries, normal intercellular canaliculi and cells appeared to be filled electron-lucent zymogen granules of varying size and density. Cells also exhibited parallel arrays of rough endoplasmic reticulum (RER) basally and laterally situated and mitochondria with normal cristae scattered throughout the cell (Figure 7A). GCT showed tall columnar cells with spherical, basally situated rounded nuclei, well circumscribed membrane bounded, electron dense secretory granules of variable size occupying the apical portion of the cells (Figure 7B). Striated duct lining exhibited tall columnar cells with vesicular, rounded nucleus and numerous, normal, rod-shaped mitochondria incorporated within the basal cell membrane infoldings that were almost parallel to the long axis of the cell. (Figure 7C).

Gp II (MTX group): Examination of the SMSG of this group showed serous cells with nuclei surrounded by irregular nuclear membrane, RER was sparse, some cells showed discontinuous RER with apical dislocation and cytoplasmic vacuoles of varying sizes were scattered throughout the cells (Figure 8A). GCTs showed shrunken nuclei with chromatin clumping surrounded by cytoplasmic vacuoles and cytoplasmic material loss. Mitochondria were mostly swollen with damaged cristae, others were ruptured (Figure 8B). Striated duct cells showed apparent loss of cell height, shrunken, pyknotic nuclei with irregular nuclear membrane and apparent loss of the typical arrangement of the mitochondria basally with loss of most of the basal infoldings of the plasma membrane. Mitochondria also showed variable grades of affection where most of them were swollen with loss of cristae, however few were constricted. (Figure 8C).

Gp III (PRP treated MTX group): Examination of the SMSG of this group showed almost normal architecture of the acini and ducts. Nuclei were basal and vesicular, surrounded by regular nuclear membrane. RER was well-developed and situated basally and laterally to the nucleus. Mitochondria were almost normal with normal shape and normal cristae. Few cytoplasmic vacuolations were seen within the cells (Figure 9A). GCTs showed basal rounded nuclei with regular nuclear membranes and almost normal mitochondria. (Figure 9B). Striated duct cells showed normal architecture with tall columnar cells having nuclei surrounded by regular membrane with finely dispersed chromatin. Numerous basal infoldings with normal mitochondria were seen dispersed in between the infoldings (Figure 9C).

Gp IV (Propolis treated MTX group): Examination of the SMSG of this group showed almost normal architecture of the acini and ducts. Nuclei were basal and vesicular with prominent nucleoli, surrounded by almost normal nuclear membrane. RER was well-developed and situated basally and laterally to the nucleus. Mitochondria were almost normal with normal shape (Figure 10A). GCTs showed rounded nuclei with regular nuclear membranes and almost normal mitochondria and normal electron dense secretory granules (Figure 10B). Striated duct cells showed normal architecture with tall columnar cells having vesicular nuclei surrounded by regular nuclear membrane with finely dispersed chromatin. Numerous, normal mitochondria were seen dispersed in between the basal infoldings, few cytoplasmic vacuolations were seen (Figure 10C).

Statistical results

There was a statistically significant difference between groups according to area percentage (%) of positive reaction to Anti-Caspase 3 with p-value ($p \leq 0.05$). The highest value was found in Gp II (4.08±0.03) followed by Gp III (0.22±0.04) then Gp IV (0.14±0.03), while the lowest value was found in Gp I (0.08±0.03) (Table 1, Figure 11).

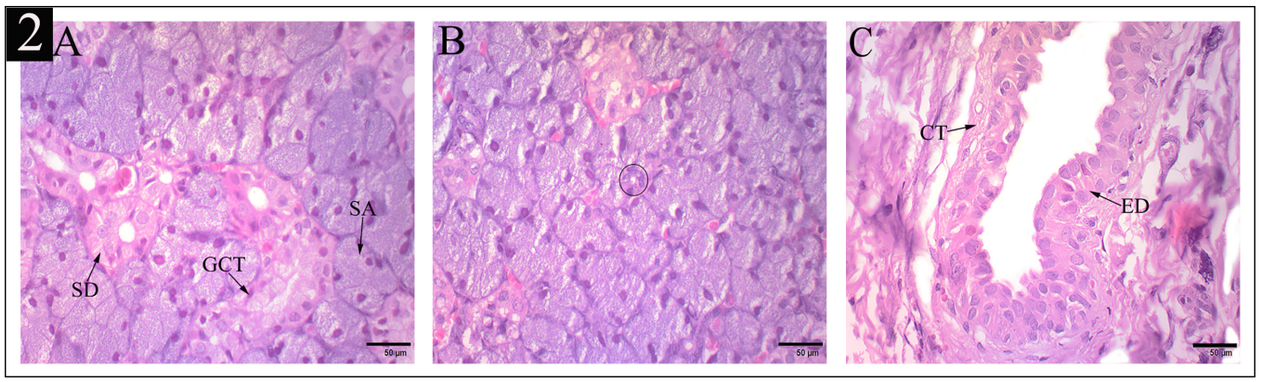

Fig. 2: Photomicrographs of the SMSG of Gp I (H&E, x400) showing: A: Serous acini with pyramidal cells, basophilic cytoplasm and basal rounded nuclei (SA), striated duct that are lined by columnar cells with centrally nuclei, eosinophilic cytoplasm and basal striations (SD), kidney shaped GCTs with apically situated eosinophilic granules (GCT). B: ICD lined by cuboidal cells and centrally placed nuclei (Circle). C: Excretory duct lined by pseudostratified columnar epithelium (ED), surrounded by fibrous CT (CT).

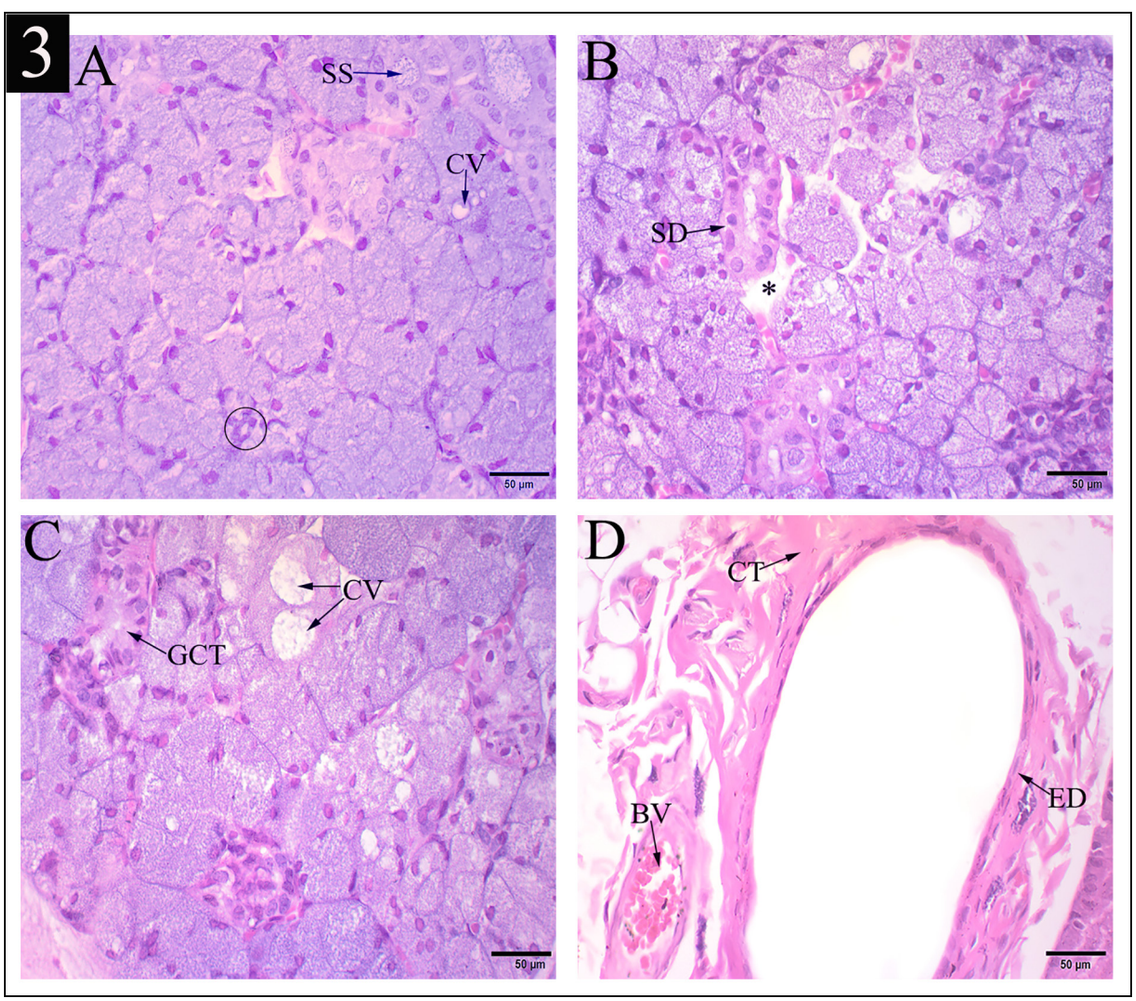

Fig. 3: Photomicrographs of the SMSG of Gp II (H&E, x400) showing: A: Serous acini showing cytoplasmic vacuolations (CV), ICD with loss of cell height (circle) and striated duct with stagnated secretion in its lumen (SS). B: Widely separated serous acini (*) and striated duct with apparent loss of basal striations (SD). C: Serous acini showing vacuolations (CV), GCT with ill-defined outline and irregular arrangement of the nuclei (GCT). D: Excretory duct with loss of pseudo-stratification with flattening of cells and nuclei (ED), hyalinized CT (CT) and congested blood vessel (BV).

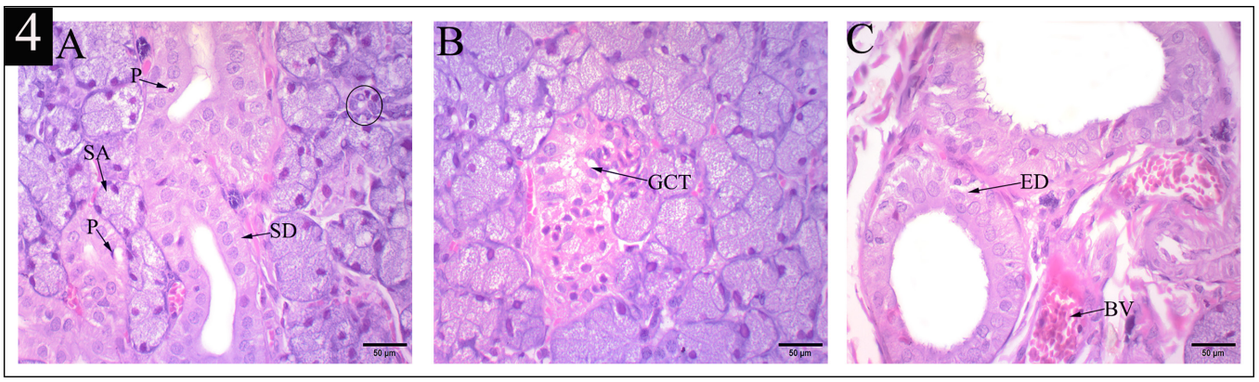

Fig. 4: Photomicrographs of the SMSG of Gp III (H&E, x400) showing: A: Serous acini (SA) and ICD (circle) appeared almost of normal architecture, striated duct appeared with basal striations (SD) and pyknotic crescent- shaped nuclei (P). B: GCTs (GCT) exhibited apparently normal outline and apical eosinophilic granules. C: Excretory duct lined by pseudostratified columnar epithelium (ED) and surrounded by congested blood vessels (BV).

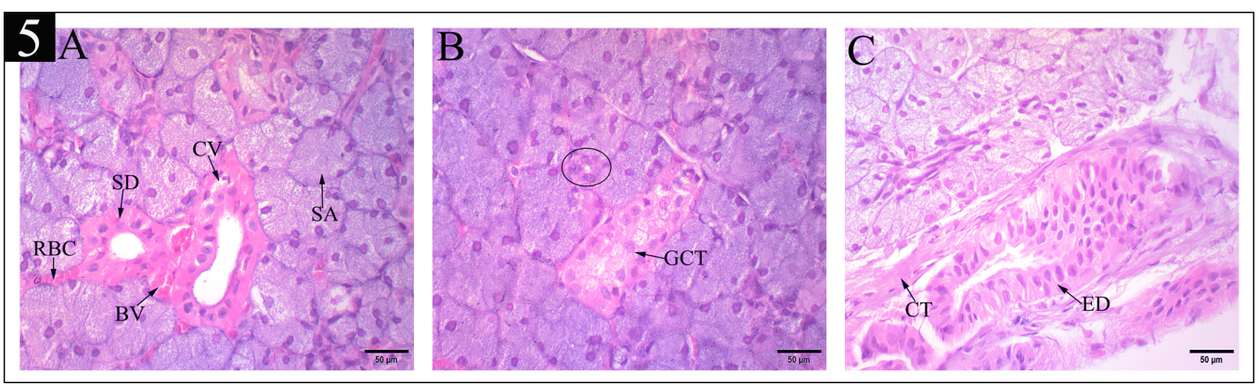

Fig. 5: Photomicrographs of SMSG of Gp IV (H&E, x400) showing: A: Serous cells (SA) with almost normal architecture, striated duct with basal striations (SD), few cytoplasmic vacuolations (CV), congested blood vessel (BV) and extravasation of RBCs (RBC). B: ICD with normal architecture (circle) and GCTs exhibited nearly normal outline with apical eosinophilic granules (GCT). C: Excretory duct with pseudostratified epithelial lining (ED) and less hyalinized CT (CT).

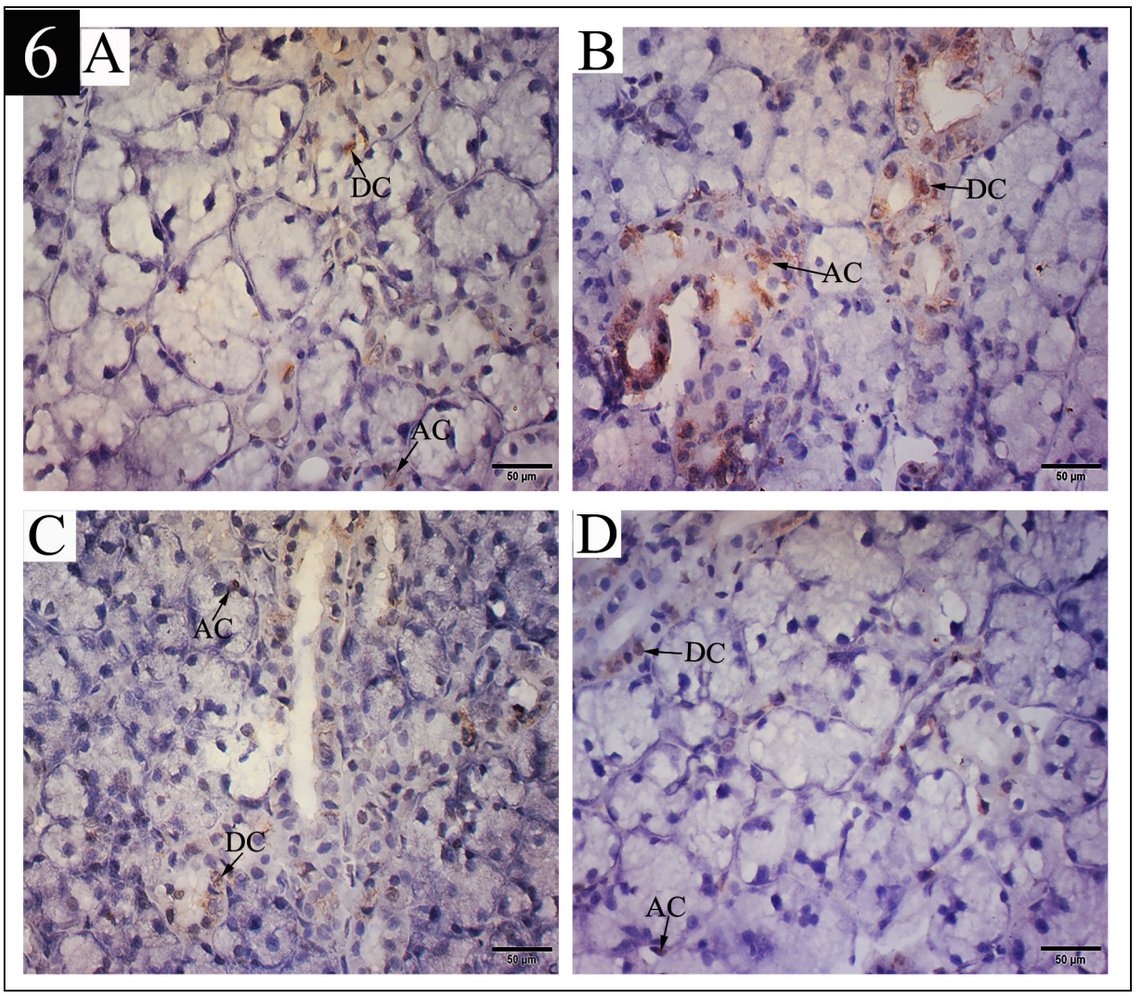

Fig. 6: Immuno-stained photomicrographs of SMSG (Anti-Caspase 3, x400). A: Gp I, B: Gp II, C: Gp III, D: Gp IV, showing; positive immunoreactivity in acinar cells (AC) and ductal cells (DC).

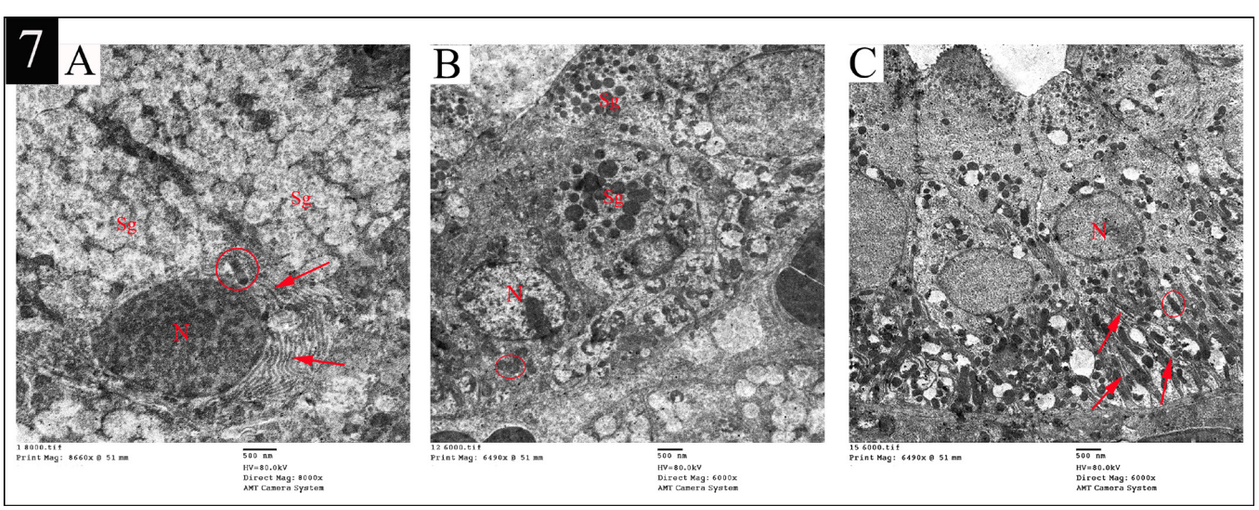

Fig. 7: Electron micrographs of SMSG from Gp I showing: A: serous acinus with basal nucleus (N) and secretory granules of varying electron densities located apically (Sg), normal RER basally and laterally (arrows) and normal mitochondria (circle) (x8000). B: GCT with normal nucleus (N), normal mitochondria (circle) and apical electron dense secretory granules (Sg) (x6000). C: Striated duct with central rounded nucleus (N), normal rod-shaped mitochondria (circle) incorporated within the basal cell membrane infoldings (arrows) (x6000).

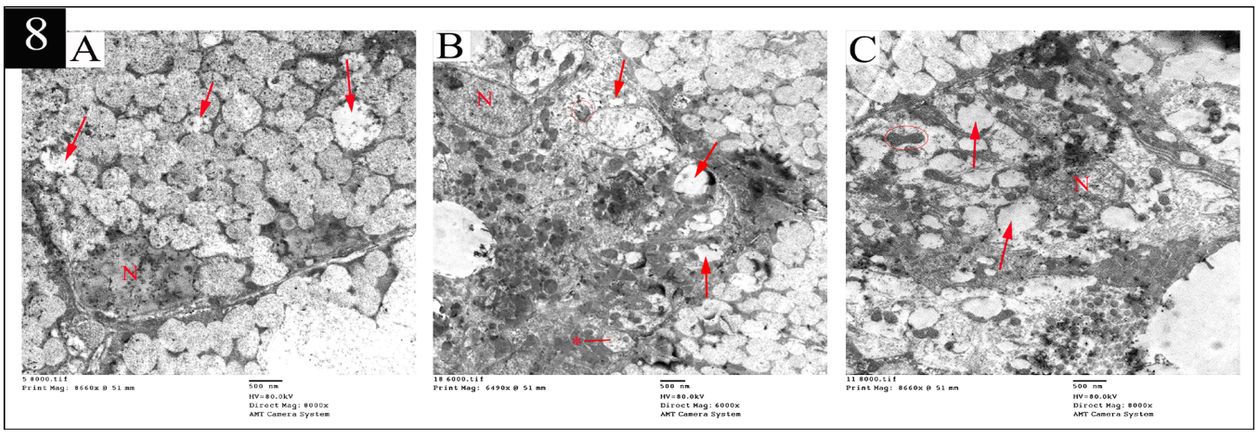

Fig. 8: Electron micrographs of SMSG from Gp II showing: A: serous cell showing nucleus with irregular nuclear membrane and chromatin clumping (N) as well as cytoplasmic vacuoles of varying sizes (arrows) (x8000). B: GCT with shrunken nucleus and chromatin clumping (N), cytoplasmic vacuolations (arrows), swollen mitochondria with damaged cristae (*), ruptured mitochondria and loss of cytoplasmic material (circle) (x6000). C: striated duct cells with pyknotic nuclei and irregular nuclear membrane (N), numerous swollen mitochondria with damaged cristae (arrows) and constricted mitochondria (circle) (x8000).

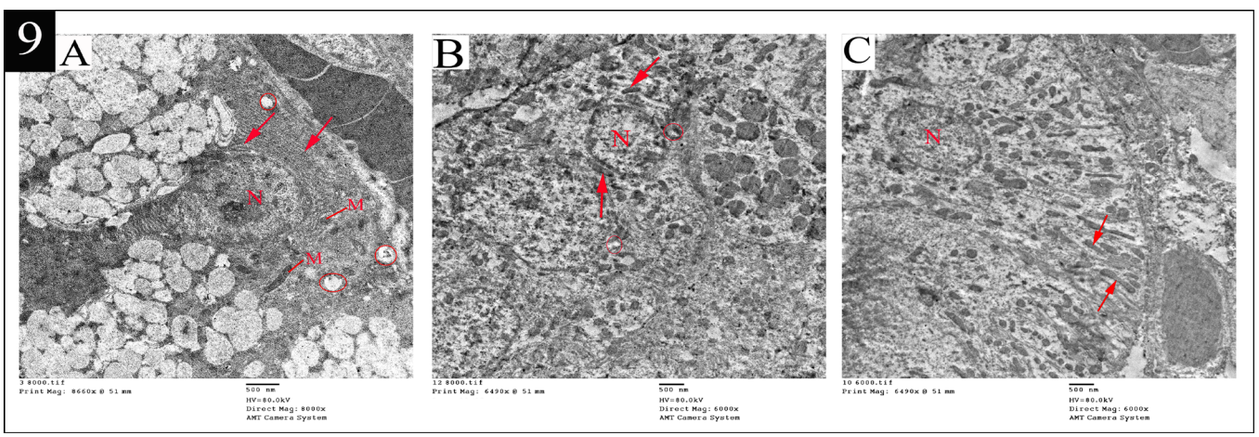

Fig. 9: Electron micrographs of SMSG from Gp III showing: A: serous cell showing basal, vesicular nucleus with regular nuclear membrane (N), parallel arrays of RER (arrows), normal mitochondria (M) and cytoplasmic vacuoles of varying sizes (circles) (x8000). B: GCT with basal rounded nucleus (N), few cytoplasmic vacuolations (circles), normal mitochondria (arrows) (x6000). C: striated duct cells with normal nucleus and regular nuclear membrane (N), numerous basally situated mitochondria with normal architecture (arrows) in between the basal infoldings (x6000).

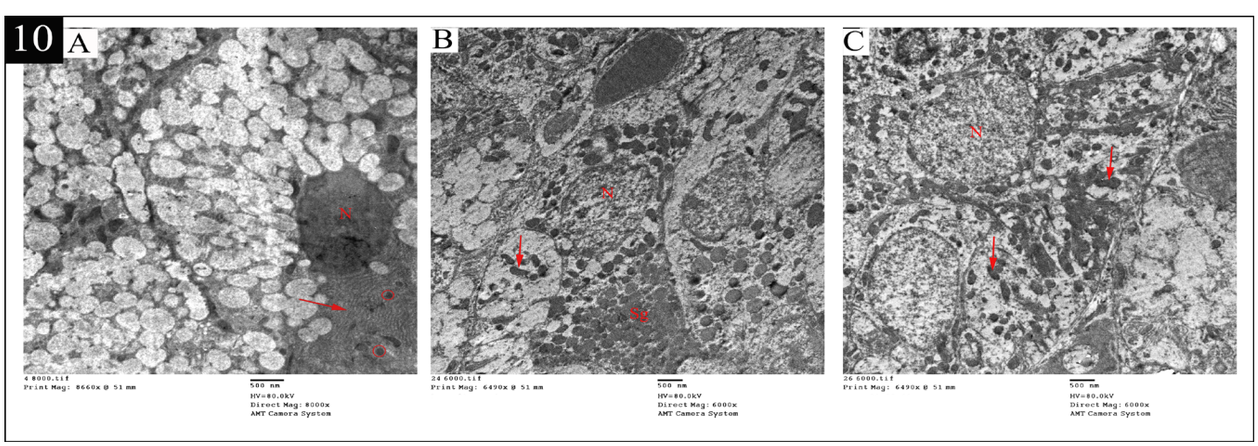

Fig. 10: Electron micrographs of SMSG from Gp IV showing: A: serous cell showing basal, vesicular nucleus with prominent nucleolus and regular nuclear membrane (N), parallel arrays of RER (arrow), normal mitochondria (circles) (x8000). B: GCT with basal rounded nucleus (N), normal mitochondria (arrow), electron dense secretory granules (Sg) (x6000). C: striated duct cells with normal nucleus and regular nuclear membrane (N), numerous basally situated mitochondria with normal architecture (arrows) (x6000).

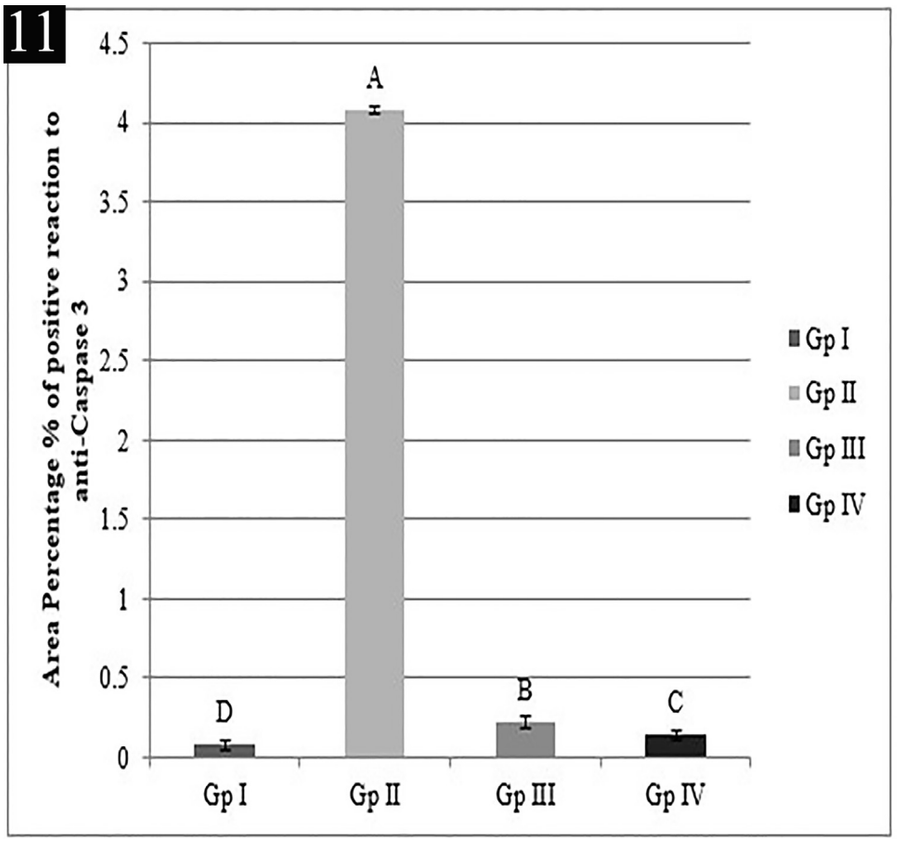

Fig. 11: Bar chart representing comparison between studied groups according to area percentage (%) of positive reaction to Anti-Caspase 3.

Table 1: Comparison between studied groups according to area percentage (%) of positive reaction to Anti-Caspase 3

Area percentage (%)	Gp I (n=7)	Gp II (n=7)	Gp III (n=7)	Gp IV (n=7)	Kruskal Wallis H-test	*p-value*
Mean ± SD	0.08 D ± 0.03	4.08 A ± 0.03	0.22 B ± 0.04	0.14 C ± 0.03	9.800	0.002*
Range	0.04 – 0.12	4.03 – 4.12	0.18 – 0.29	0.1 – 0.19		

*: Significant at $P < 0.05$, Values in row which have different superscripts are significantly different.

DISCUSSION

MTX is a chemotherapeutic agent used in treatment of several types of cancers as well as many inflammatory diseases. However, many experimental studies have demonstrated that MTX has deleterious effects on different body tissues. These effects are mainly resulted from generation of free radicals and ROS, leading to lipid peroxidation and mitochondrial impairment which has been an important cause of oxidative damage to cells[25,26]. The selected dose of MTX in the existing experiment was (80 mg/Kg) similar to[3] that investigated different MTX doses on SMSG, showing that there was an increase in the cytotoxic effect by increasing the dose of MTX and the maximum toxic effects were observed in rats treated by (80 mg/Kg) after 48 h.

In the current study, PRP was chosen to ameliorate the damaging effects of MTX as the previous studies of[27,28] documented that PRP is the portion of blood plasma that is enriched with platelets and considered to be a compound of various growth factors and bioactive substances. These factors orchestrate tissue regeneration and accelerate soft tissue healing.

In the present study, Propolis was used as it is considered a potent antioxidant and a free radical scavenger, reducing the generation of oxidative stresses[29,30]. It was proven in the study of[31] that using antioxidant supplements allows patients to tolerate higher effective doses of chemotherapy and improve survival rate.

Anti-Caspase 3 was chosen in this research as an immunohistochemical marker for detecting the apoptotic cells. A previous study of[32] investigated that MTX leads to activation of the mitochondrial apoptotic pathway through mitochondrial release of cytochrome C, activation of Caspase 9 which induces executioner Caspase 3 activation, leading to cell degradation and apoptosis.

In the current study, the histology of SMSG of Gp II showed degenerative changes in form of atrophy with some nuclei of the acinar and ductal cells appeared hyperchromatic and pyknotic as seen in the results of[3].

These findings were supported ultra-structurally in our experiment by the presence of shrunken, dark acinar and ductal nuclei with irregular nuclear membranes which agree with the results of[4], examining the effect of MTX on parotid gland. These findings could be attributed to MTX-induced apoptosis that was statistically confirmed in our study by a highly significant increase in area percentage of positive reaction to Anti-Caspase 3 compared to Gp I which come in accordance with[33], investigating MTX degenerative effects on kidneys.

Numerous cytoplasmic vacuolations of varying sizes were revealed in the acinar and ductal cells of Gp II of the present study, examined by both LM and TEM which are consistent with the research of[4,29] attributed these vacuoles to the released free radicals which caused damage to the cellular components. Moreover,[34] explained the occurrence of vacuolations as one of the primary responses to all forms of cell injury. In our study, the vacuolations in the parenchymal elements might be due to swollen mitochondria with damaged cristae that being shown mainly in ductal cells by TEM examination. This explanation is in accordance with[35].

In the current study, LM results of the duct system of Gp II showed further changes in form of apparent loss of cell height, GCTs appeared disfigured with irregular arrangement of their nuclei, striated ducts revealed loss of basal striations and loss of pseudo-stratifications of excretory ducts. Ultra-structurally, Striated ducts showed ruptured and damaged mitochondria with loss of its typical arrangement as well as loss of most of the basal infoldings, demonstrating the loss of basal striations seen by LM. These findings are in parallel with that of[2] and could be contributed to MTX-induced degeneration of these cells. The variable grades of affection of mitochondria as constricted, condensed with increased matrix density and others appeared swollen with loss of matrix density that detected ultra-structurally in our results of the ducts of GP II explained by[36] as a consequence of free radicals and ROS generation.

In the existing study, Gp III revealed few pyknotic nuclei and cytoplasmic vacuolations in the acini and ducts. Striated ducts appeared with basal striations, and excretory ducts showed pseudostratified appearance. On the TEM level, there were many vesicular nuclei, almost normal mitochondria, well organized RER in acinar and ductal cells. Striated duct cells showed normal architecture with numerous basal infoldings which illustrated the LM picture of ducts of this group. These results, regarding the curative effects of PRP, are in consistence with[10] who documented an obvious improvement in the morphology of the pancreatic tissue in the diabetic animals after PRP treatment. As well as,[37] reported that PRP appeared to be effective in regeneration of SMSG architecture after severe irreversible atrophic changes with almost normal architecture of serous acini and ducts with few cytoplasmic vacuolization. Furthermore, lithium and PRP-treated group in the study of[11] exhibited significant amelioration of thyroid follicular cell changes occurred due to Lithium toxicity.

The capability of PRP to reduce MTX induced salivary gland damage histologically and ultra-structurally was explained by[8,9,38]. The researchers reported the fact that PRP has a natural cocktail of growth factors and bioactive substances. These growth factors include, epidermal growth factor, platelet derived growth factor, Vascular endothelial growth factor, transforming growth factor-β1, connective tissue growth factor and fibroblast growth factor. These factors enhance tissue healing and regeneration, supporting our results.

Moreover, there was a statistically significant decrease in the area percentage of positive reaction to Anti-Caspase 3 in Gp III compared to Gp II. This finding was supported by[28] who documented that PRP has anti-apoptotic activities through downregulating the expression of apoptotic genes as well as inhibiting Caspase 3 levels.

In this research, SMSG of Gp IV revealed superior histological and ultrastructure improvement that found nearly same as illustrated in Gp I. Also, GP IV showed the statistically significant least area percentage of positive reaction to Anti-Caspase 3 when compared to Gp II and Gp III. These results agree with[19] who reported that propolis has a powerful antioxidant property and is capable of modulating the activities of antioxidant enzyme as well as suppresses the oxidative damage that induced by MTX in liver and brain tissues. In addition,[30] documented that propolis prevented the increase in apoptotic cells number using TUNEL assay and improved kidney morphology in rats received MTX.

Several studies related the powerful antioxidant effect of Propolis to the high content of total phenolics, flavonoids as caffeic acid phenethyl ester and dihydroflavanols found in Propolis. These compounds scavenge free radicals and prevents lipid peroxidation, decreasing the MTX-induced damage to different tissues[39,40].

In the present study, both PRP and Propolis have therapeutic value in ameliorating the degenerative effects of MTX on SMSG. Both treatments were comparable to each other, however propolis gave better results than PRP. This was based on the more detected improvements in Gp IV than Gp III. Further investigations are required with longer experimental periods, co-administration of PRP with Propolis and increase the dose or repeated administration of PRP.

CONCLUSIONS

PRP and propolis treatment reduced the detrimental effects of MTX on SMSG with more improvements were achieved in propolis than PRP treated group.

ABBREVIATIONS

CT, connective tissue; **DAB,** diaminobenzidine plus chromogen; **GCT,** granular convoluted tubule; **H&E,** Hematoxylin & Eosin; **ICD,** intercalated duct;

LM, light microscope; **MTX,** methotrexate; **PBS,** phosphate buffered saline; **PPP,** platelet poor plasma; **PRP,** platelet rich plasma; **ROS,** reactive oxygen species; **RBCs,** red blood cells; **rpm,** revolution per minute; **RER,** rough endoplasmic reticulum; **SD,** standard deviation; **SMSG,** submandibular salivary glands; **TEM,** transmission electron microscope.

CONFLICT OF INTERESTS

There are no conflicts of interest.

REFERENCES

1. Harvey RA: Anticancer Drugs: In Lippincott's illustrated reviews: Pharmacology: 5th ed., Lippincott Williams & Wilkins a Wolters Kluwer business, Baltimore (2012) pp: 301-315.
2. Omar AI, Yousry MM and Farag EA: Therapeutic mechanisms of granulocyte-colony stimulating factor in methotrexate-induced parotid lesion in adult rats and possible role of telocytes: A histological study. Egy. J. Histol. (2018) 41 (1): 93-107.
3. Al-Refai AS, Khaleel AK and Ali S: The Effect of Green Tea Extract on Submandibular Salivary Gland of Methotrexate Treated Albino Rats: Immunohistochemical Study. J. Cytol. Histol. (2014) 5: 2.
4. Abd El-Fatah SS, Yousef DM and Al-Semeh AE: Oxidative Stress Changes Induced by Methotrexate on Parotid Gland Structure of Adult Male Albino Rat: Can Vitamin C Ameliorate These Changes? Med. J. Cairo Univ. (2019) 87 (4): 2555-2565.
5. Duan WR, Garner DS, Williams SD, Funckes-Shippy CL, Spath I. and Blomme E.G: Comparison of immunohistochemistry for activated caspase-3 and cleaved cytokeratin 18 with the TUNEL method for quantification of apoptosis in histological sections of PC-3 subcutaneous xenografts. J. Pathol. (2003) 199 (2): 221-228.
6. Lopez-Vidriero E, Goulding KA, Simon DA, Sanchez M and Johnson DH: The Use of Platelet-Rich Plasma in Arthroscopy and Sports Medicine: Optimizing the Healing Environment. Arthroscopy: The Journal of Arthroscopic and Related Surgery (2010) 26 (2): 269-278.
7. Tschon M, Fini M, Giardino R, Filardo G, Dallari D, Torricelli P, Martini L, Giavaresi G, Kon E, Maltarello MC, Nicolini A. and Carpi A: Lights and shadows concerning platelet products for musculoskeletal regeneration. Frontiers in bioscience (2011) 3 (1): 96-107.
8. Cavallo C, Roffi A, Grigolo B, Mariani E, Pratelli L, Merli G, Kon E, Marcacci M and Filardo G: Platelet-Rich Plasma: The Choice of Activation Method Affects the Release of Bioactive Molecules. Biomed. Res. Int. (2016) 2016: 6591717.
9. Pavlovic V, Ciric M, Jovanovic V and Stojanovic P: Platelet Rich Plasma: a short overview of certain bioactive components. Open Med. (2016) 11 (1): 242-247.
10. El-Tahawy NF, Rifaai RA, Saber EA, Saied SR and Ibrahim RA: The effect of Platelet Rich Plasma (PRP) Injection on the Endocrine Pancreas of the Experimentally Induced Diabetes in Male Albino Rats: A Histological and Immunohistochemical Study. J. Diabetes Metab. (2017) 8 (3): 730.
11. El-Mahalaway AM and El-Azab NE: Impacts of resveratrol versus platelet-rich plasma for treatment of experimentally lithium-induced thyroid follicular cell toxicity in rats. A histological and immunohistochemical study. Ultrastructural pathol. (2019) 43 (1): 80-93.
12. Ozcan P, Takmaz T, Tok OE, Islek S, Yigit EN and Ficicioglu C: The protective effect of platelet-rich plasma administrated on ovarian function in female rats with Cy-induced ovarian damage. J. Assist. Reprod. Genet. (2020) 37: 865-873.
13. Luzo ACM, Favaro WJ, Seabr AB and Duran N: What is the potential use of platelet-rich-plasma (PRP) in cancer treatment? A mini review. Heliyon (2020) 6 (3): e03660.
14. Cihan YB and Baykan H: The effect of platelet rich plasma on radiotherapy. Turk. J. Biochem. (2021) 46 (1): 9-12.
15. Hemieda FAE, El-Kholy WM, El-Habibi EM and El-Sawah SG: Influence of propolis on oxidative stress, inflammation and apoptosis in streptozotocin-induced diabetic rats. IJAR (2015) 3 (7): 831-845.
16. Anjum SI, Ullah A, Khan KA, Attaullah M, Khan H, Ali H, Bashir MB, Tahir M, Ansari MJ, Ghramh HA, Adgaba N and Dash CK: Saudi J. Biol. Sci. (2019) 26 (7): 1695-1703.
17. Mahmoud MF and Sakr SM: Hepatoprotective Effect of Bee Propolis in Rat Model of Streptozotocin-Induced Diabetic Hepatotoxicity: Light and Electron Microscopic Study. Life Sci. J. (2013) 10 (4): 2048-2054.
18. Al-Saeed HF and Mohamed NY: The Possible Therapeutic Effects of Propolis on Osteoporosis in Diabetic Male Rats. Nat. Sci., (2015) 13 (3): 136-140.
19. Khalil FA, EL-Kirsh AAA, Kamel EA and EL-Rahmany NG: Beneficial effect of propolis extract (bee glue) against methotrexate-induced stress in liver and brain of albino rats. Indian j. med res. pharm. Sci. (2016) 3 (6): 24-34.
20. Abu Almaaty AH, Abd El-Aziz YM, Omar NA, Abdeen AM, Afifi H, Ibrahim TS, Elhady SS and Khedr AIM: Antioxidant Property of the Egyptian Propolis ExtractVersus Aluminum Silicate Intoxication on a Rat's Lung: Histopathological Studies. Molecules (2020) 25 (24): 5821.

21. National Research Council (US) Committee for the Update of the Guide for the Care and Use of Laboratory Animals: Guide for the care and use of laboratory animals. (8th ed.). National Academy Press, Washington (2011) pp: 41-196.

22. Bancroft JD, Suvarna K and Layton C: Bancroft's theory and practice of histological techniques. (7th ed.). Churchill Livingstone: Elsevier (2013) pp: 173-186.

23. Edebali N, Tekin IÖ, Açıkgöz B, Açıkgöz S, Barut F, Sevinç N and Sümbüloğlu V: Apoptosis and necrosis in the circumventricular organs after experimental subarachnoid hemorrhage as detected with annexin V and caspase 3 immunostaining. Neurol. Res. (2014) 36 (12): 1114-1120.

24. Korany NS and Ezzat BA: Prophylactic effect of green tea and Nigella sativa extracts against fenitrothion-induced toxicity in rat parotid gland. Arch. Oral Biol. (2011) 56 (11): 1339-1346.

25. Tousson E, Atteya Z, El-Atrash A and Jew-Eely OI: Abrogation by Ginkgo Byloba Leaf Extract on Hepatic and Renal Toxicity Induced by Methotrexate in Rats. J. Cancer Res. Treat. (2014) 2 (3): 44-51.

26. Arpag H, Gül M, Aydemir Y, Atilla N, Yiğitcan B, Cakir T and Sayan M: Protective Effects of Alpha-Lipoic Acid on Methotrexate-Induced Oxidative Lung Injury in Rats. J. Invest. Surg. (2018) 31 (2): 107-113.

27. Okuda K, Kawase T, Momose M, Murata M, Saito Y and Suzuki H: Platelet-Rich Plasma Contains High Levels of Platelet-Derived Growth Factor and Transforming Growth Factor- β and Modulates the Proliferation of Periodontally Related Cells In *Vitro*. J. Periodontol. (2003) 74 (6): 849-857.

28. Jia C, Lu Y, Bi B, Chen L, Yang Q, Yang P, Guo Y, Zhu J, Zhu N and Liu T: Platelet-rich plasma ameliorates senescence-like phenotypes in a cellular photoaging model. RSC Adv. (2017) 7(6): 3152-3160.

29. Conklin KA: Chemotherapy-Associated Oxidative Stress: Impact on Chemotherapeutic Effectiveness. Integr. Cancer Ther. (2004) 3 (4): 294-300.

30. Ulusoy HB, Ismet Ozturk I and Sonmez MF: Protective effect of propolis on methotrexate-induced kidney injury in the rat. Renal Failure (2016) 38 (5): 744-750.

31. Singh K, Bohri M, Kasu YA, Bhat G and Ma-Rar T: Antioxidants as precision weapons in war against cancer chemotherapy-induced toxicity-Exploring the armoury of obscurity. Saudi Pharma., J. (2018) 26 (2018): 177-190.

32. Natarajan K, Abraham P and Kota R: Activation of the mitochondrial apoptotic pathway contributes to methotrexate-induced small intestinal injury in rats. Cell Biochem. Funct. (2017) 35 (7): 378-391.

33. Aidaros AE, Shehata MA, Abdelfatah MT and Kamel AM: Effects of Methotrexate and Vitamin C on Renal Cortex of Rats. Int. j. pharm. res. allied sci. (2018) 7 (4): 137-151.

34. Suriyakumari KVP, Udayakumar R and Ruba T: Histological investigations on kidney of sildenafil citrate (edegra) treated albino mice. Int. J. Anat. Res. (2016) 4 (1): 1977-1980.

35. Lombaert IM, Brunsting JF, Wierenga PK, Kampinga HH, De Haan G and Coppes RP: Cytokine treatment improves parenchymal and vascular damage of salivary glands after irradiation. Clin. Cancer Res. (2008) 14 (23): 7741-7750.

36. Solenski NJ, diPierro CG, Trimmer PA, Kwan AL, Gregory A and Helms GA: Ultrastructural Changes of Neuronal Mitochondria After Transient and Permanent Cerebral Ischemia. Stroke (2002) 33(3): 816-824.

37. Anwar S, Yahia W and Gaballah O: Effect of Platelet Rich Plasma on Regeneration of Submandibular Salivary Gland of Albino Rats. N. Y. Sci J. (2018) 11 (12): 27-40.

38. Halpern B, Chaudhury S and Rodeo S: The role of platelet-rich plasma in inducing musculoskeletal tissue healing. HSSJ. (2012) 8 (2): 137-145.

39. Cakır T, Ozkan E and Dulundu E: Caffeic acid phenethyl ester (CAPE) prevents methotrexate-induced hepatorenal oxidative injury in rats. J. Pharm. Pharmacol. (2011) 63 (12): 1566-1571.

40. Salem MM, Donia T, Abu-Khudira R, Ramadan H, Ali EMM and Mohamed TM: Propolis Potentiates Methotrexate Anticancer Mechanism and Reduces its Toxic Effects. Nutrition and Cancer (2020) 72 (3): 460-480.

الملخص العربى

الدور التحسيني المحتمل للبلازما الغنية بالصفائح الدموية مقابل البروبوليس على الأضرار المحدثة بعقار ميثوتركسيت في الغدد اللعابية تحت الفكية للذكور البالغة من الفئران البيضاء (دراسة بإستخدام المجهر الضوئي والإلكتروني النافذ)

رانيا أسامة محمد محسن، هند المسيري

قسم بيولوجيا الفم ـ كلية طب الاسنان ـ جامعة عين شمس

الخلفية: العلاج الكيميائي هو أحد التدخلات الرئيسية لعلاج السرطان. لسنوات عديدة، يتم إستخدام عقار ميثوتركسيت كعلاج كيميائي فعال. ولكن عقار ميثوتركسيت له تأثيرات سامة على الغدد اللعابية مسببا خللاً وظيفياً بها. البلازما الغنية بالصفائح الدموية هي طريقة علاجية جديدة. وهي مصدر قوي يستخدم في إصلاح الأنسجة. أما بالنسبة للمنتجات الطبيعية مثل البروبوليس فهو يعتبرآداة طبية بديلة لها تأثير كبير على صحة الإنسان.

هدف الدراسة: هو فحص تأثير البلازما الغنية بالصفائح الدموية مقابل البروبوليس على الغدد اللعابية تحت الفكية للفئران التي تلقت عقار ميثوتركسيت.

طرق و مواد البحث: أستخدم ثمانية وعشرين فئرا أبيضا من الذكور البالغة وقسموا إلى أربع مجموعات متساوية. المجموعة الضابطة: لم تتلق الفئران أي أدوية. مجموعة عقار ميثوتركسيت (Gp II): تم حقن الفئران بجرعة واحدة داخل الصفاق من عقار ميثوتركسيت (٨٠ مجم / كجم). مجموعة عقار ميثوتركسيت المعالجة بالبلازما الغنية بالصفائح الدموية (Gp III): حقنت الفئران بعقار ميثوتركسيت كالمجموعة ((Gp II ، ثم بعد ٤٨ ساعة ، حقنت الفئران بحقنة واحدة تحت الجلد من البلازما الغنية بالصفائح الدموية (٠,٥ مل / كجم). مجموعة عقار ميثوتركسيت المعالجة بالبروبوليس (Gp IV): حقنت الفئران بعقار ميثوتركسيت كالمجموعة Gp) (II، ثم بعد ٤٨ ساعة ، أعطيت الفئران عن طريق الفم جرعة يومية واحدة من البروبوليس (٣٠٠ مجم / كجم) معلقة في ١ مل من الماء المقطر. بعد ستة أيام من حقن عقار ميثوتركسيت تم التضحية بالفئران بشكل منفصل بجرعة زائدة من المخدر ثم تم تشريح الفئران وتحضير الغدد اللعابية تحت الفكية للفحص بالمجهر الضوئي و الإلكتروني النافذ.

النتائج: أظهر الفحص بالمجهر الضوئي و الإلكتروني النافذ أن أنسجة الغدة تحت الفكية للفئران التي حقنت بعقار ميثوتركسيت أظهرت تغيرات واضحة; كظهور العديد من الفراغات السيتوبلازمية ، تعدد شكل أنوية الخلايا، تغيرات إنتكاسية في شكل ضمور و فصل بين الحويصلات. كما أظهرت القنوات تغيرات إنتكاسية واضحة. أظهرت المجموعة المعالجة بعقار ميثوتركسيت في التحليل الإحصائي تغيرات في النسبة المئوية للتفاعل الإيجابي مع Anti-Caspase ٣ مقارنة بـالمجموعة الضابطة. في المجموعات المعالجة ، أظهرت مجموعة عقار ميثوتركسيت المعالجة بالبلازما الغنية بالصفائح الدموية و مجموعة عقار ميثوتركسيت المعالجة بالبروبوليس في الغدد اللعابية تحت الفكية تحسينات نسيجية واضحة مع انخفاض ملحوظ في النسبة المئوية للتفاعل الإيجابي مع Anti-Caspase ٣ مقارنة بـالمجموعة المعالجة بعقار ميثوتركسيت.

الإستنتاجات: أظهرت هذه الدراسة أن إعطاء البلازما الغنية بالصفائح الدموية والبروبوليس مع عقار ميثوتركسيت له إستراتيجية علاجية فعالة في تحسين التأثيرات الضارة لعقار ميثوتركسيت على الغدد اللعابية تحت الفكية.